NUMERICAL AND EXPERIMENTAL STRUCTURAL ANALYSIS OF UNMANNED AERIAL VEHICLE WINGS

Flávio Luiz de Silva Bussamra, flaviobu@ita.br
Carlos Miguel Montestruque Vilchez, cmontes@ita.br
Júlio César Santos, julio@ita.br
ITA – Instituto Tecnológico de Aeronáutica, Divisão de Engenharia Aeronáutica
Praça Marechal Eduardo Gomes, 50 - CEP 12228-900 – São José dos Campos – SP – Brasil.

Abstract. *This paper presents the methodology used to analyze the structural behavior of the wing of an unmanned aerial vehicle (UAV). This UAV is a prototype aircraft made of ply wood, balsa wood and aluminum, with a wingspan of 2,5m. Numerical and experimental analyses are presented and performed. A finite element model is proposed to numerically analyze this wing. Also, an experiment is proposed to apply static symmetrical maneuvers loads to the wings. Experimental and numerical data, like displacements, strains and failure modes are compared and discussed.*

Keywords*: Unmanned aerial vehicle, structural analysis, experimental analysis, numerical analysis, UAV.*

1. INTRODUCTION

An Unmanned Aerial Vehicle – UAV – is a remotely controlled or autonomous aircraft, meaning that it is operated without a flight crew member on board. This class of aircraft is useful in situations where it is too dangerous or too expensive to use manned aircraft.

Since the beginning of 2005, the *Instituto de Engenharia Aeronáutica* – ITA, São José dos Campos-SP, Brazil, has been developing an UAV, sponsored by *Financiadora de Estudos e Projetos* – FINEP, with the partnership of *Centro de Estudos Avançados do Recife* – CESAR – and *Companhia Hidro-Elétrica do São Francisco* - CHESF.

The main objective of this project is the development of an UAV capable of inspecting electrical transmission lines, with reliability. Nowadays, this inspection is made by helicopters, typically with one pilot and a technician filming or taking pictures.

The UAV requirements are:

- cruising speed: 120 km/h;
- capability to fly at 80 km/h up to 160 km/h;
- capability to fly at 1000m above sea level;
- capability to take off and landing in rough fields, like grass or vicinal roads;
- landings and take-offs are not automatic, and will be conducted by humans, with remote control, like aero models;
- the UAV must carry a camera to film the power lines. In order to minimize image vibrations, the camera must be fixed near the center of gravity of the airplane;
- flight range in the preliminary project: 40 km;
- the power lines must be inspected (filmed) at horizontal distance of 25m and vertical distance of 30 m;
- the UAV must automatic follow the power lines using on-board computers (automatic pilot) and GPS technology.

In this UAV Project, a prototype is being developed, constructed and tested. The main objective of this project is to verify whether a small aircraft, subjected to gust loads, will be capable of filming with suitable quality the power lines. In this “proof of concept”, aspects like long range, durability or maintenance were much less important than low costs and rapid and easy construction. So, the airplane structure of the prototype is made of balsa wood and ply wood. Further versions will possibly be made of composite materials. Electronic hardware will be acquired and integrated on the airplane.

Girardi and Rizzi (2006, 2005a, 2005b) presented the methodology used to design the UAV, witch main characteristics of the UAV are shown in Table 1.

Another platforms rather than airplane were considered (Girardi and Rizzi, 2005c), like helicopters or zeppelins, but the airplane seemed to be the most suitable option.

Table 1. Main characteristics of the UAV.

Parameter	
Wing area (S)	0.883 m^2
Wing span (b)	2.486 m
Wing chord (C_w)	0.355 m
Aileron chord (C_A)	0.071 m
Maximum take off weight (MTOW)	206 N
Limit positive load factor	4.4
Ultimate positive load factor	6.6
Limit negative load factor	-2.2
Ultimate negative load factor	-3.3

2. WOOD MECHANICAL PROPERTIES

In order to determinate the mechanical properties of the balsa wood and plywood in tension (Young's modulus and maximum tensile stress), a series of tensile tests were conducted.

The specimen dimensions were based upon (ASTM D 3500, 2003), with some adaptations when necessary to adequate available samples, noting that small section bars were used. Figure 1 shows pictures of the test in balsa sheet and the grips used. Electrical strain-gages by Measurements Group, Inc., CEA-13-250UW-120, were used.

Specific masses were determined by using (ASTM D 2395, 2002) Standards.

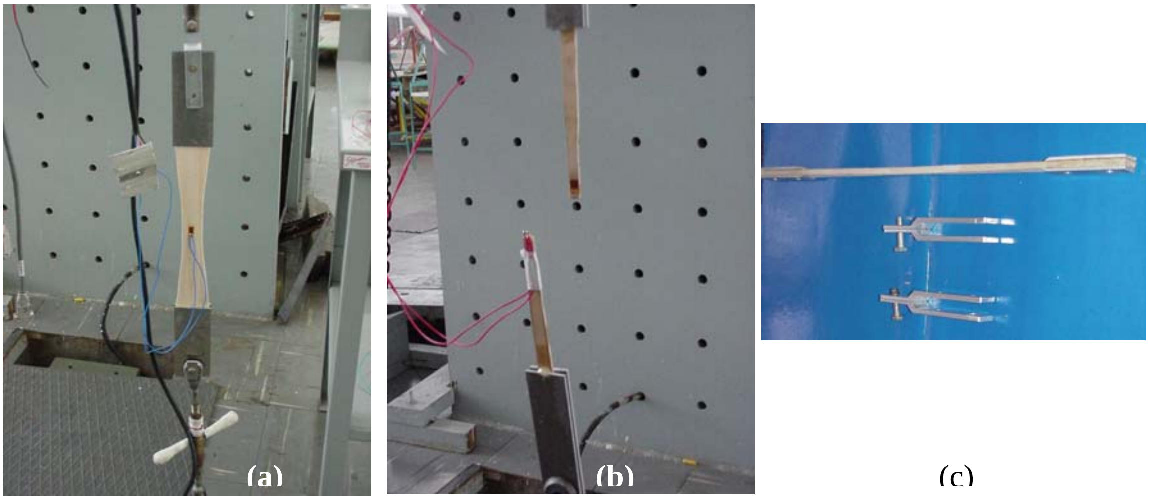

Figure 1 – Tension tests: a) balsa sheet; b) balsa bar; c) grips.

A typical stress strain curve is shown in Fig. 2, for a tension test in balsa bar sample of rectangular cross section of 6 mm x 15 mm. All tests showed that balsa wood is very fragile in tension, and nonlinearities were not observed.

Figure 3 shows the relationship between specific mass and tensile strength and Young's Modulus.

Material mechanical data adopted in this work are presented in Table 2, where E is the average Young Modulus (assumed identical in tension and compression), S_t is the rupture stress in tension (average minus the standard deviation), and S_c is the rupture stress in compression (assumed as 0,7 S_t); ρ is the specific mass.

3. WING STRUCTURE

3.1 Loads

According to US regulation code FAR Part23 (CFR, 2005), "strength requirements are specified in terms of limit loads (the maximum loads to be expected in service) and ultimate loads (limit loads multiplied by prescribed factors of safety). Unless otherwise provided, prescribed loads are limit loads. (…) Unless otherwise specified, a factor of safety of 1.5 must be applied to the prescribed limit load."

An important question that arises is:: what code is suitable to UAV? All international codes are applied to aircraft with pilot. US code FAR Part23 (CFR, 2005) is applied to "normal", "utility", "acrobatic" and "commuter" airplane. The European code (Anon., 2003a) is applied to very light airplanes, and (Anon. 2003b) is applied to sailplanes and powered sailpanes.

The European code (Anon, 2003a), applied to very light airplanes, is adopted in this project, where prescribed limits load factor are listed in Tab 3.

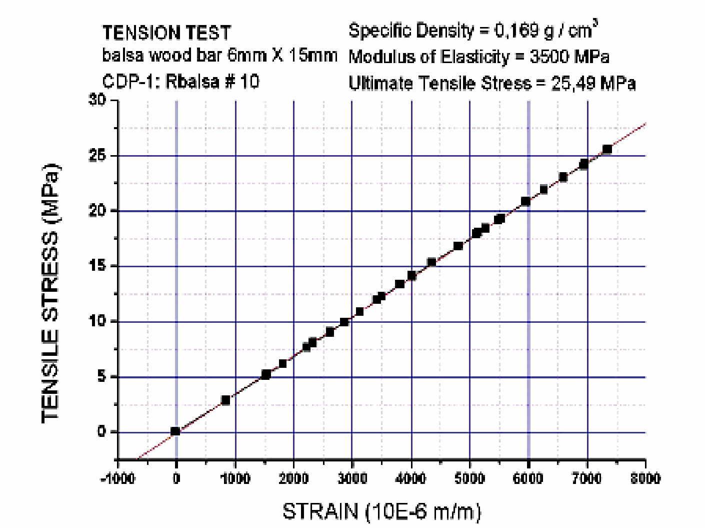

Figure 2 – Typical stress-strain curve for balsa wood bar.

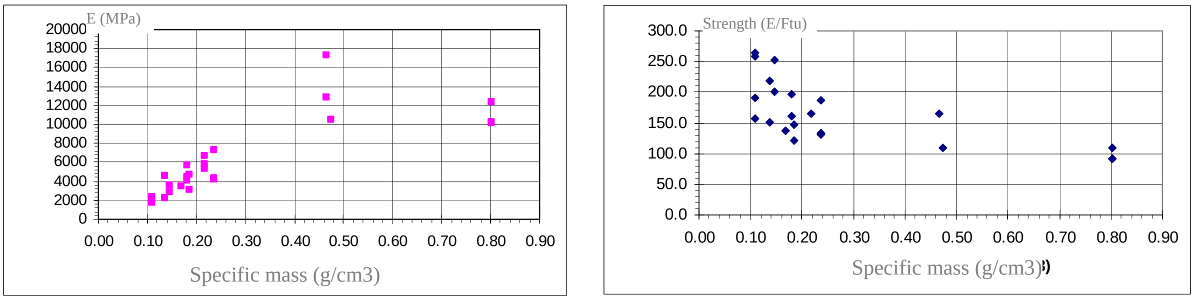

Figure 3 – Young's modulus and strength *vs*. specific mass in balsa wood bar.

Table 2. Mechanical properties along fiber direction.

	E (GPa)	S_t (MPa)	S_c (MPa)	ρ (Kg/m^3)
Balsa wood bar	4,8	26	18	200
Balsa wood sheet	2,0	7,4	5,2	110
Ply wood sheet	6,0	70	49	500

Table 3 – Load factors for symmetric maneuvers

Condition	Maximum positive load factor	Maximum negative load factor
Limit	4.4	-2.2
Ultimate	6.6	-3.3

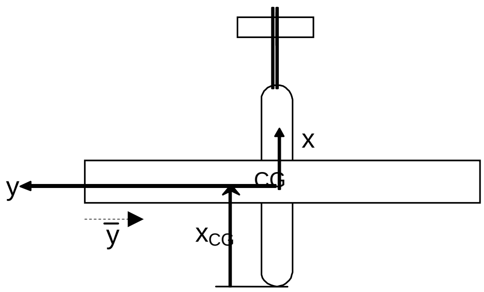

Figure 4 – UAV body axes.

Figure 4 presents the aircraft body axes. Real lift load q_z is approximately an ellipse curve Shear load S_z and bending moment M_x can be found by integrating q_z, according to eqs. 1 and 2:

$$S_z(\bar{y}) = \int_0^{b/2} q_z(\bar{y})d\bar{y} \tag{1}$$

$$M_x(\bar{y}) = \int_0^{b/2} S_z(\bar{y})dy \tag{2}$$

To simplify the integrations above (eqs. 1 and 2), the distributed load was fitted by a cubic polynomial. Figure 5a presents the design distributed ultimate load and the fitted curve; Figures 5b and 5c show the ultimate shear load and ultimate bending moment, applied to the left wing, in symmetric maneuver, and also, it can be seen the loads applied in structural tests (see item 3.3).

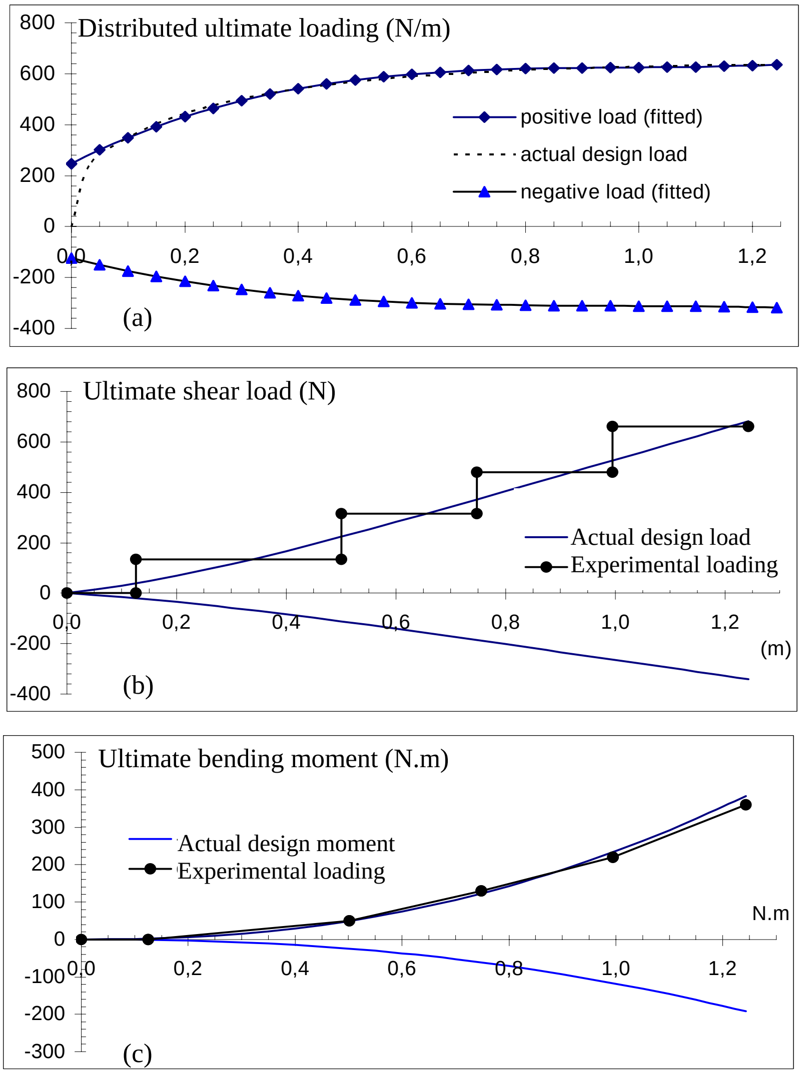

Figure 5 – Ultimate design load and testing loads.

3.2 Wing design and construction

The wing structure was divided in two different sections, shown in Figs. 6 and 7. The first one (root section) extends from the airplane axe (symmetric plane) to y = 0.353 m, i.e., this section has a total length of 0.646 m. The second section (tip section) extends from the end of root section to the tip of the wing, with 0.90 m of length each side. It may be noticed that, at the transition of the mid and tip sections, the bending moment is M_x = 197 N.m, approximately half the maximum bending moment at the root (M_x = 406 N.m). The wing is made of balsa wood, except the longeron and the skin of the root section, made of ply wood. Cyanoacryllic and epoxi glues were used to connect bars and skin.

Figure 7 also shows the location of the 8 strain-gages and 4 displacement transducers used in the experimental tests. Strain gages D1 to D6 were fixed at balsa stringer bars; AS1 and AI1 were fixed at balsa upper and lower skins, respectively.

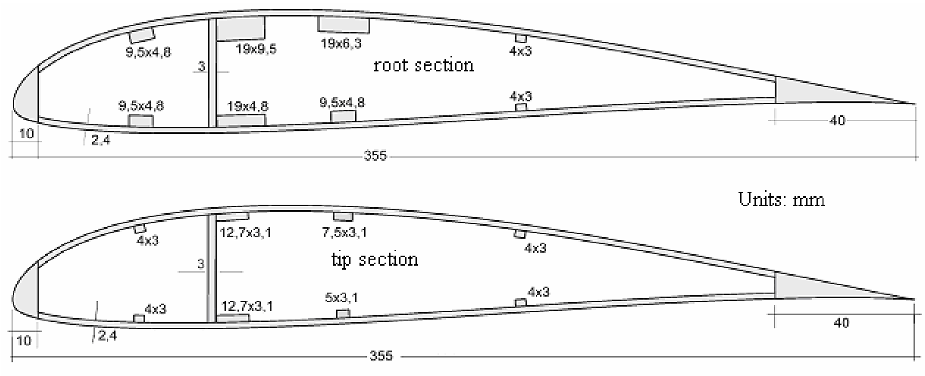

Figure 6 – Wing structural cross sections.

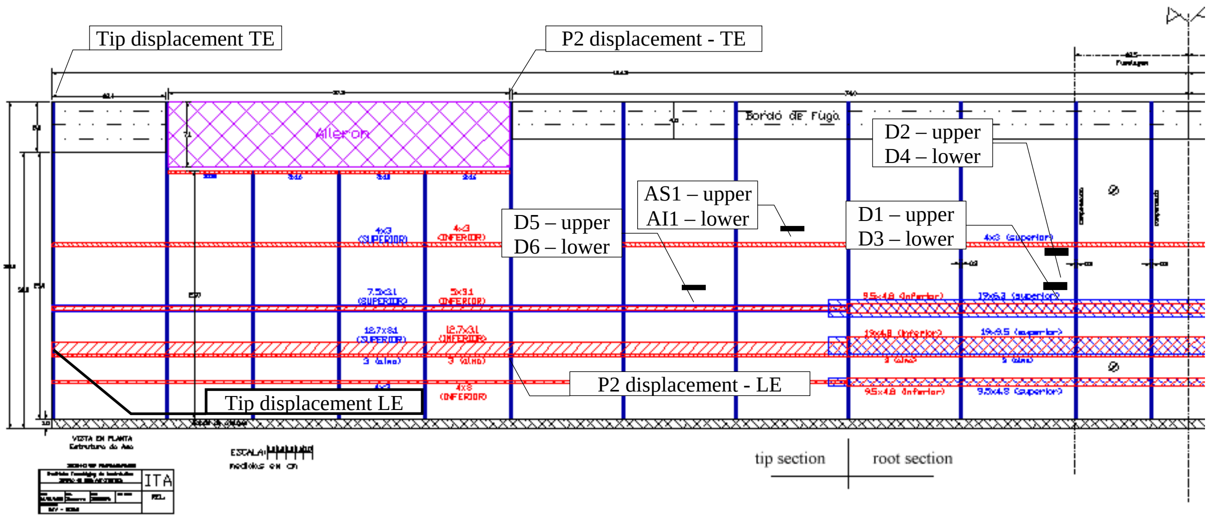

Figure 7 – UAV right wing design and strain gages and displacement transducers.

3.3 Finite Element Modeling

MSC/Nastran (MSC, 2002) finite element software was used to analyze the wing. Balsa bars were modeled by 2-node linear rod elements; skin was modeled by 4-node plate element, with membrane capabilities, and the longeron was modeled by parabolic plate element, also with membrane capabilities. The model has 846 degrees of freedom.

Figure 8 shows the deformed wing and normal stresses in the wing skin.

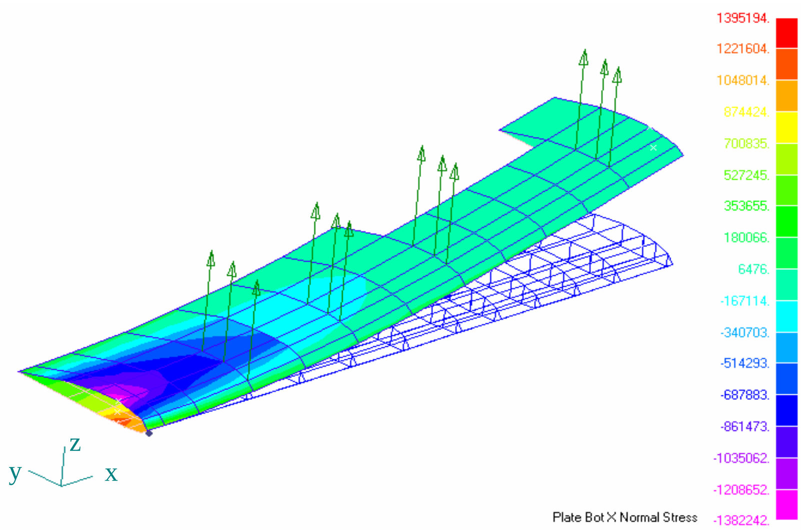

Figure 8 – Finite element model for the right wing. Displacements and normal stress in the skin.

3.4 Wing experimental tests

Figure 9 shows a picture of the experimental setup. Loads were measured by load cell transducer. A load tree was used to distribute the total load to four sections each side (see Fig. 5). Load steps of about 44.5 N (10 lbf) were applied on each branch of the tree.

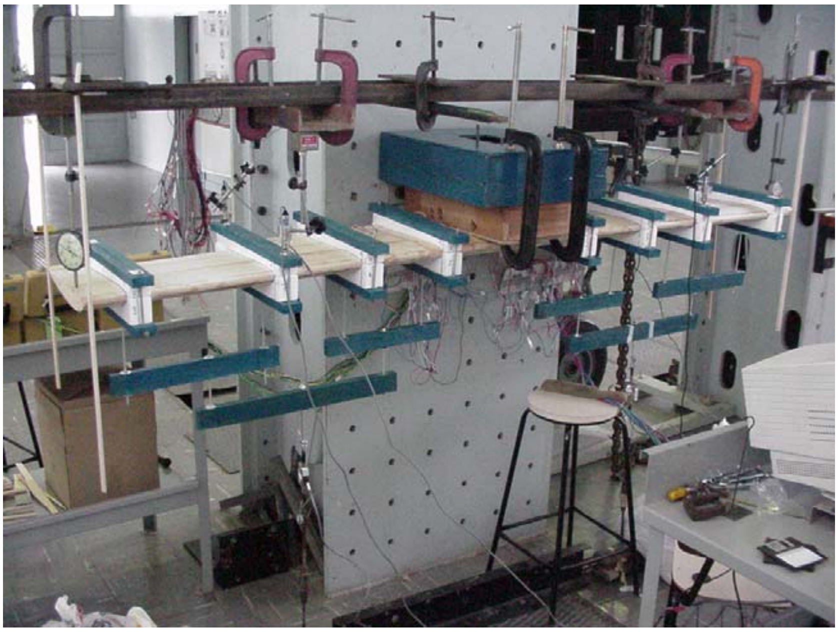

Figure 9 – Experimental setup of the static load test.

Two displacements gages were fixed at left wing tip. Figure 10 shows load *versus* finite element model and experimental displacements. It can be noticed that experimental measurements P2 were limited to 9 mm. Displacements plotted at Fig. 10 are the average between the leading edge and trailing edge displacements.

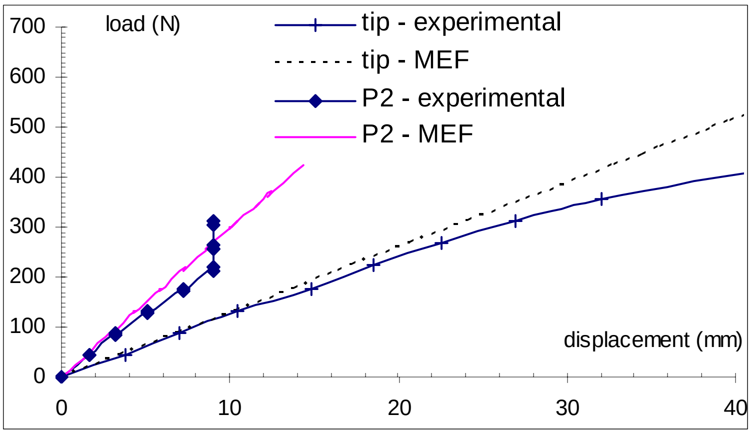

Figure 10 – Experimental and finite element displacements.

Eight strain-gages were at each left and right wings. Strain-gages D1, D2 and D5 were fixed at upper balsa bars, D3, D4 and D6 at lower bars, and strain-gages AS1 and AI1 were fixed at upper and lower skins, respectively (see Fig. 7). Figure 11 shows total load *versus* experimental strains and the finite element model strains.

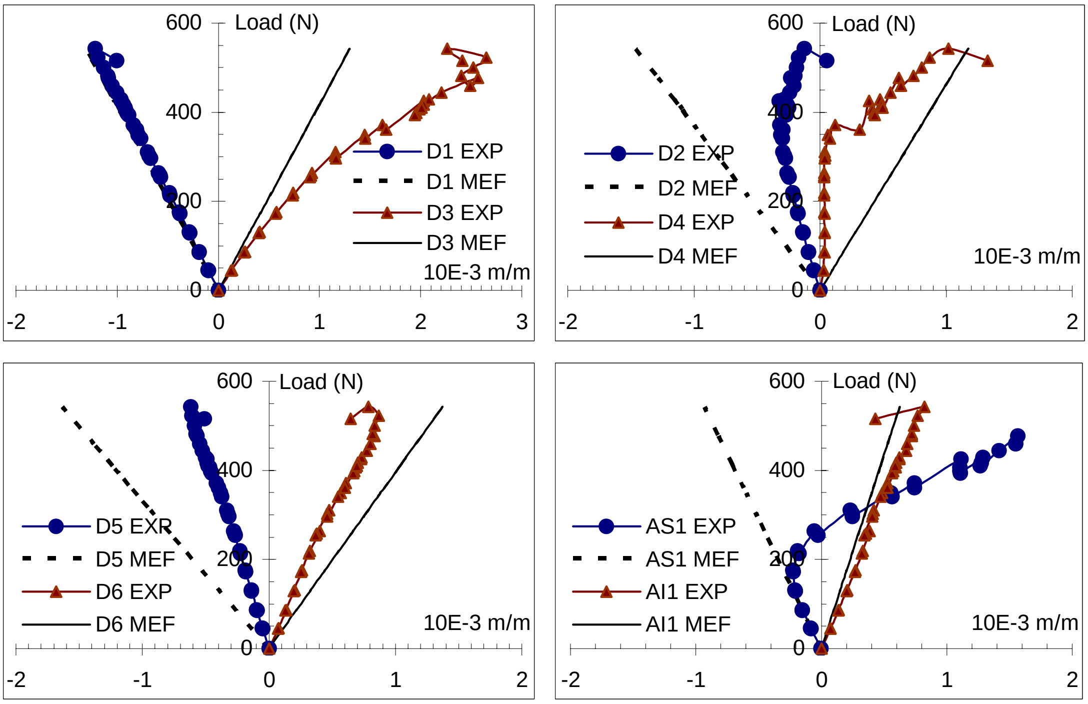

Figure 11 – Experimental and finite element model strains.

Finite element model gave accurate predictions for displacements, and for D1, D3 AS1 and AI1 strains, at least in the linear phases.

Misbehave of strain gage AS1 indicated the local buckling of the upper skin panel. Strain gages D2 and D4 did not give accurate results, probably because of the proximity of the rib.

Figure 12 shows a picture of the right wing at 622 N (140 lbf). This load, equivalent to 91% of the ultimate design load (680N), was the maximum load applied at the right wing, when the upper skin buckled (it can be noticed that wing was mounted upside-down). Figure 13 shows the failure of the upper skin.

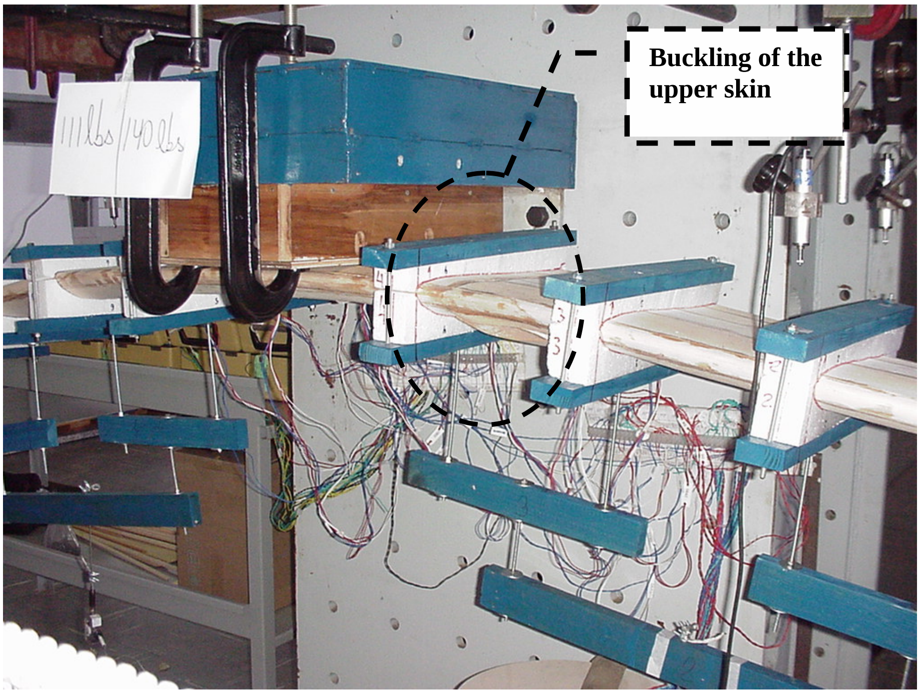

Figure 12 – Maximum load applied to the right wing.

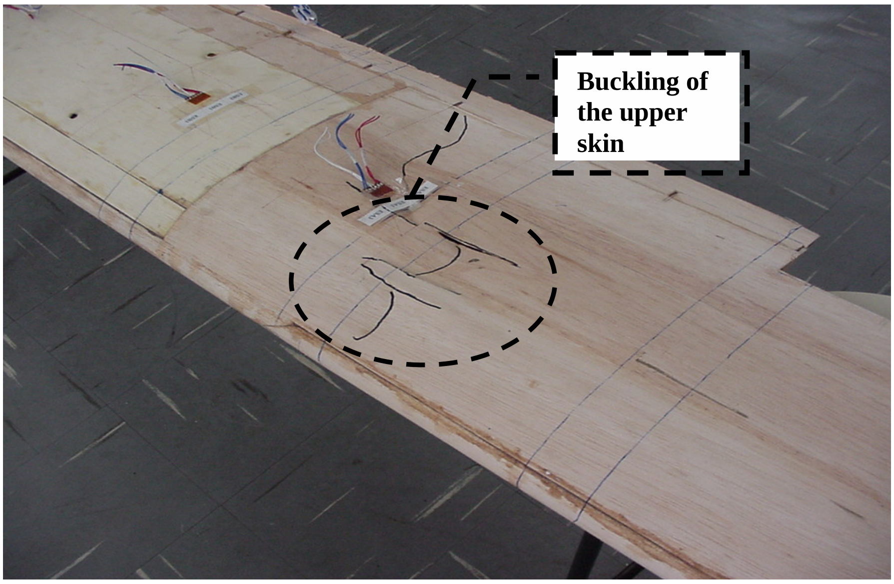

Figure 13 – Buckling failure at 91% of ultimate load (622 N).

None of the stringer bars, nor the longeron were damaged.

The left wing supported a maximum load of 494 N (111 lbf), 73% of ultimate load. The failure was caused by the ungluing of the upper skin, followed by a sudden buckling of the upper skin.

3.4. Reinforcements

Due to the buckling failure of the upper skin, each wing was reinforced with three more wing ribs. The previous structure had 12 ribs each half-wing (Fig. 7), while the re-designed half-wing has 15 ribs (Fig. 14), more concentrated in the transition of plywood skin and balsa wood skin.

Also, special attention was taken with the gluing process.

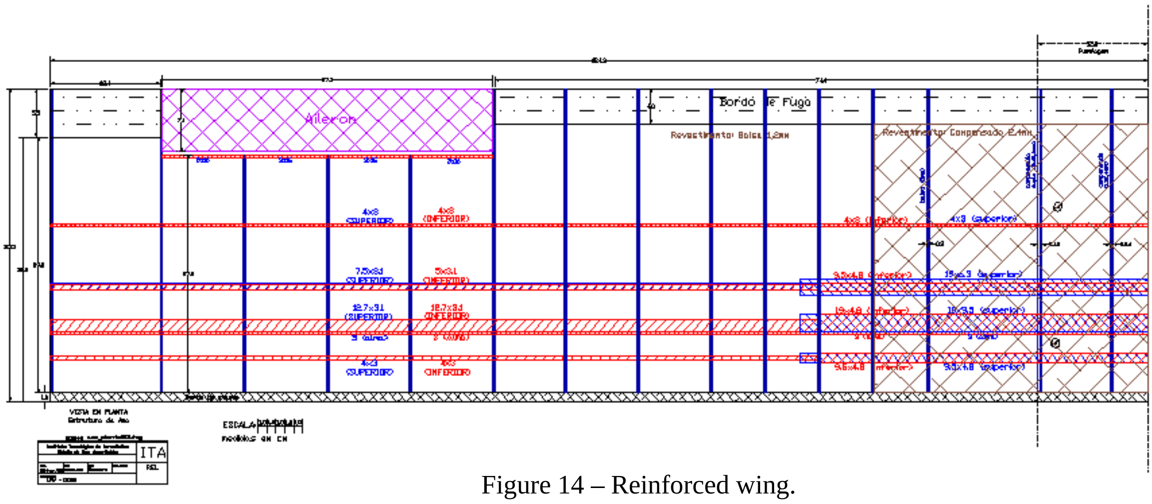

Figure 14 – Reinforced wing.

The final structural design of the UAV is shown in Figure 15.

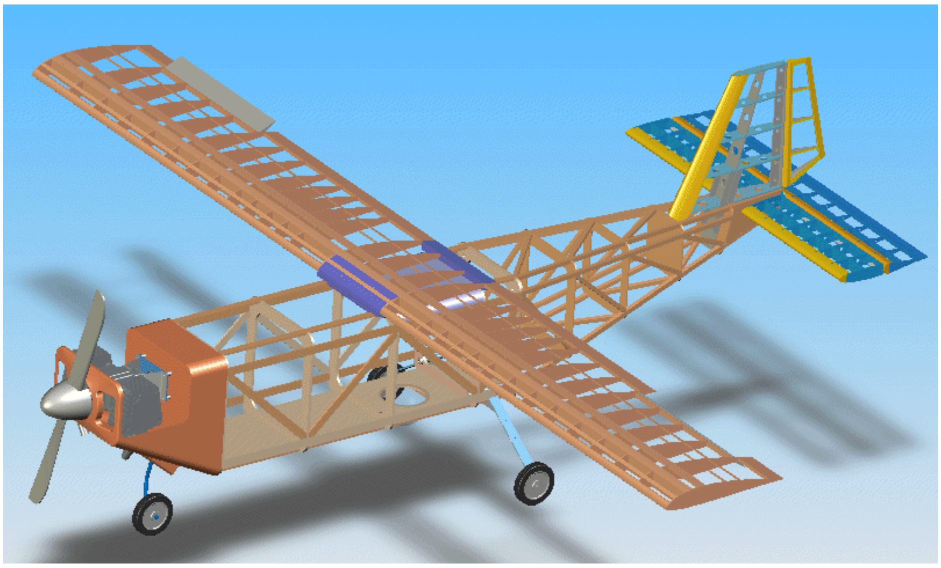

Figure 15 – Framework of the UAV.

4. CONCLUSIONS

The finite element analysis was used to analyze the wing structure, giving support data for its design. Tension tests were developed to determine mechanical properties of balsa wood and ply wood. A wing was built and structural tests were performed.

Displacements were predicted with very good accuracy during the elastic phase. As the finite element model was linear, the non-linear behavior was not predicted. Some strains were predicted with good accuracy, others were not. In further structural wood wing tests, attention to interferences must be taken in account when locating strain gages.

The left wing supported the total design load, with 9% of margin of safety, but supported 73% of ultimate load. Problems with the glue seem to have caused the failure. The right wing supported the total design load with 37% of margin of safety, but supported 91% of ultimate load. Buckling of upper balsa wood skin caused the failure.

These results gave support to design reinforcements in the wing. Also, the assemblage and gluing process seem to be critical, and changes to the construction process were made.

To enhance the capability of predicting the failure behavior by using finite element modeling, it is important to determine the mechanical behavior of the wood in compression and shear loading.

The methodology presented in this work will be used for the construction of the second prototype, with longer flight range. The use of wood or fabric is still in discussion.

5. ACKNOWLEDGEMENTS

The authors would like to thank the FINEP-Financiadora de Estudos e Projetos, CESAR-Centro de Estudos Avançados do Recife and CHESF-Companhia Hidro-Elétrica do São Francisco.

6. REFERENCES

Anon. (2003a), *Certificatuin Specifications for Very Light Aeroplanes CS-VLA*, European Aviation Safety Agency, Decision no. 2003/18/RM, nov/14/2003.

Anon. (2003b), *Certification Specifications for Sailplanes and Powered Sailplanes CS-22*, European Aviation Safety Agency, Decision no. 2003/13/RM, nov/14/2003.

ASTM Standards D 2395 – (2002), "*Standard Test Methods for Specific Gravity of Wood and Wood-Based Materials*", ASTM International.

ASTM Standards D 3500 – 90 (2003), "*Standard Test Methods for Structural Panels in Tension*", ASTM International.

Code of Federal Regulations, Title 14, Volume 1, Revised as of January 1, 2005, From the U.S. Government Printing Office via GPO Access[CITE: 14CFR23], Page 165-339, Title 14--AERONAUTICS AND SPACE, CHAPTER I--FEDERAL AVIATION ADMINISTRATION, DEPARTMENT OF TRANSPORTATION, PART 23_AIRWORTHINESS STANDARDS: NORMAL, UTILITY, ACROBATIC, AND COMMUTER CATEGORY AIRPLANES, accessed on 10/25/2005.

Girardi, R.M., Rizzi,P., 2006. Desenvolvimento de Metodologia para projeto conceitual de um veículo aéreo não tripulado (VANT), usado para inspeção de linhas de transmissão de energia elétrica. *IV Congresso Nacional de Engenharia Mecânica, CONEM 2006*, Anais, Recife, Brazil, 2006 (in print).

Girardi,R.M., Rizzi,P. et alli, 2005a, *Projeto conceitual da aeronave, utilizando métodos de cálculo que fornecem boas estimativas, em tempo reduzido, dos parâmetros que definem a aeronave*, Relatório de trabalho, CESAR/ITA, 20 de dezembro, Brazil. (in portuguese).

Girardi,R.M., Rizzi,P.,2005b, *Análise do tipo de aeronave mais adaptada para a inspeção de linhas de transmissão*, Relatório de trabalho, CESAR/ITA, 27 de junho, Brazil. (in portuguese).

Girardi,R.M., Rizzi,P.,2005c, *Seleção da alternativa mais promissora para prova de conceito, através da construção e testes em vôo*, Relatório de trabalho, CESAR/ITA, 27 de junho, Brazil. (in portuguese).

MSC Software Corporation, *MSC Nastran 2001, Quick Reference Guide, USA, 2002.*

7. RESPONSIBILITY NOTICE

The authors are the only responsible for the printed material included in this paper.